Theoretical analysis of resonant inelastic x-ray scattering spectra in $LaMnO_3$

Taeko Semba,[1] Manabu Takahashi,[2] and Jun-ichi Igarashi[1]
[1]*Faculty of Science, Ibaraki University, Mito, Ibaraki 310-8512, Japan*
[2]*Faculty of Engineering, Gunma University, Kiryu, Gunma 376-8515, Japan*
(Received 24 June 2008; revised manuscript received 3 September 2008; published 13 October 2008)

We analyze the resonant inelastic x-ray scattering (RIXS) spectra at the *K* edge of Mn in the antiferromagnetic insulating manganite $LaMnO_3$. We make use of the Keldysh-type Green's function formalism, in which the RIXS intensity is described by a product of an incident-photon-dependent factor and a density-density correlation function in the 3*d* states. We calculate the former factor using the 4*p* density of states given by an *ab initio* band-structure calculation and the latter using a multiorbital tight-binding model. The ground state of the model Hamiltonian is evaluated within the Hartree-Fock approximation. Correlation effects are treated within the random-phase approximation (RPA). We obtain the RIXS intensity in a wide range of energy loss (2–15 eV). The spectral shape is strongly modified by the RPA correlation, showing good agreement with the experiments. The incident-photon-energy dependence also agrees well with the experiments. The present mechanism that the RIXS spectra arise from band-to-band transitions to screen the core-hole potential is quite different from the orbiton picture previously proposed, enabling a comprehensive understanding of the RIXS spectra.

DOI: 10.1103/PhysRevB.78.155111 PACS number(s): 78.70.En, 75.47.Lx, 71.28.+d, 78.20.Bh

I. INTRODUCTION

Recently, the perovskite-type manganites showing the colossal magnetoresistance (CMR) effect have attracted much attention because the CMR effect may be the key for high-capacity magnetic storage and spintronics as next-generation electronic devices. It is widely recognized that the spin, charge, and orbital degrees of freedom of the 3*d* electrons play important roles in the CMR effect in the manganites. In the undoped material $LaMnO_3$, the crystal structure[1,2] belongs to the *Pbnm* space group below 780 K, where each MnO_6 octahedron is noticeably rotated, tilted, and distorted due to the cooperative Jahn-Teller distortion (JTD).[3] The orbital degeneracy in the e_g states is lifted by the JTD or by the orbital exchange interaction similar to the superexchange for spins,[4] forming an orbital-ordered state, in addition to an *A*-type antiferromagnetic (AFM) long-range order.[5,6] With hole doping, a variety of spin, charge, and orbital-ordered phases appear. It is widely accepted that the CMR effect is a consequence of the destruction of the orbital-ordered state in the presence of a magnetic field, which may break the subtle balance among the multiple degrees of freedom.

Resonant inelastic x-ray scattering (RIXS) technique using the x ray tuned at the transition-metal *K* edge has been recognized as a powerful tool to investigate the charge and orbital degrees of freedom in transition-metal compounds. The RIXS process is described as a second-order optical process, in which a 1*s*-core electron is excited to an empty 4*p* state by absorbing an incident photon, then charge excitations are created in the 3*d* states to screen the core-hole potential, and finally the photoexcited 4*p* electron recombines with the 1*s*-core hole by emitting a photon. In the final state, the charge excitations are left behind in the 3*d* states. In contrast to the optical conductivity measurement, it allows us to investigate the momentum dependence of the excitations because the corresponding x rays have wavelengths of the same order of lattice spacing. The clear momentum dependence has been observed in cuprates.[7–11] Note that electron-energy-loss spectroscopy can also detect the momentum dependence, but it cruelly suffers from multiple scattering effects.

Several RIXS experiments have been carried out on $LaMnO_3$ and the hole-doped compounds.[12–14] For the undoped case, the RIXS spectra show three noticeable features at the energy loss 2.5, 8, and 11 eV, when the incident-photon energy is tuned near the Mn *K* edge.[12] These features are also observed in the hole-doped manganites.[13,14] Based on the theoretical analysis exploiting the Liouville operator method,[15] Inami *et al.*[12] argued that the 2.5 eV peak arises from an orbital excitation across the Mott gap, which is driven by the off-diagonal part of the Coulomb interaction between a photoexcited 4*p* electron and an e_g electron. This assumption, however, seems unrealistic, because such an off-diagonal Coulomb interaction is much smaller than the Coulomb interaction between the 1*s* hole and 3*d* electrons. This mechanism could not explain the origin of the 8 and 11 eV peaks either. The purpose of this paper is to elucidate the origin of the observed features in the RIXS spectra of $LaMnO_3$ on the basis of the well-established assumption that the charge excitations are created in the 3*d* states to screen the core-hole potential. To obtain the comprehensive understanding of the spectra, we use a multiorbital tight-binding model involving all the Mn 3*d* orbitals and O 2*p* orbitals, and take account of the crystal distortion forming *Pbnm* by varying the transfer energy between the 3*d* and 2*p* orbitals.

We calculate the RIXS intensity with the use of the formula proposed by Nomura and Igarashi (NI).[16,17] The NI formula of the RIXS spectra is a kind of extension of the resonant Raman theory developed by Nozières and Abrahams[18] on the basis of the many-body formalism of Keldysh.[19] The formula has advantages that it can rather easily be applied to complicated models including many orbitals and provides clear physical interpretations of the RIXS spectra. This formula utilizes the Born approximation to the core-hole potential, and divides the RIXS intensity into two fac-

tors; one describes an incident-photon dependence and the other is the density-density correlation function in the 3*d* states. Similar formulas have been derived by using different methods.[20] The NI formula has been successfully applied to the quasi-one-dimensional cuprates $SrCuO_3$,[16] $CuGeO_3$,[9] two-dimensional cuprate La_2CuO_4,[17,21,22] and the prototypical AFM insulator NiO.[23] In these studies, the calculations have been carried out at zero temperature; the electronic structures in the AFM phase have been calculated within the Hartree-Fock approximation (HFA). It is known that the HFA works well for the description of electronic structures in the AFM insulators. Two-particle correlations have been taken into account within the random-phase approximation (RPA). It has been found that the RPA correction modifies strongly the spectral shape as a function of energy loss, having led to a good agreement with the experiments. With these successes, we may conclude that the RIXS intensity arises from band-to-band transitions to screen the core-hole potential in the intermediate state. Multiple-scattering contributions due to the core-hole potential have been also investigated in order to examine the validity of the Born approximation, because the core-hole potential is not definitely weak.[21] Having evaluated the contributions by means of the time-representation method by Nozières and De Dominicis,[24] it was found that the contributions could be mainly absorbed into the shift of the core-level energy with minor modifications of the RIXS spectral shape.[21] This result partly justifies the use of the Born approximation.

In the present study of $LaMnO_3$, we treat the strong Coulomb interaction between the 3*d* orbitals within the HFA; we obtain an *A*-type AFM insulating solution with an energy gap ~ 1.0 eV, where the occupation on the $3z^2-r^2$-type orbital is larger than that on the x^2-y^2-type orbital at each Mn site. This result corresponds well to the observed orbital-ordered state. Note that the band-structure calculation with the local-density approximation (LDA) fails to reproduce the wide energy gap. We calculate the density-density correlation function at zero temperature by using the energy bands thus obtained and by treating the two-particle correlations within the RPA. We calculate another factor, the incident-photon-dependent factor, using the 4*p* density of states (DOS) obtained from the *ab initio* band-structure calculation. Combining the two factors, we finally obtain the RIXS spectra, which show good agreement with the experiments.[12–14] We could assign the 2.5 eV peak in the RIXS spectra as a function of energy loss to the electron-hole excitation across the Mott gap in local majority spin channel, and the 8 (11) eV peak to the transition from the occupied e_g states strongly hybridized with the O 2*p* states in the deep valence band to the unoccupied e_g states in the local majority (minority) spin channel. We also make clear the origin of the incident-photon dependence of the spectra by examining the corresponding factor in our formula.

The present paper is organized as follows. In Sec. II A, we introduce the multiorbital tight-binding model. In Sec. II B, we discuss the electronic structure within the HFA in the AFM phase of $LaMnO_3$. In Sec. III, we briefly summarize the NI formula for the RIXS spectra. In Sec. IV, we present the calculated RIXS spectra in comparison with the experiments. Section V is devoted to the concluding remarks.

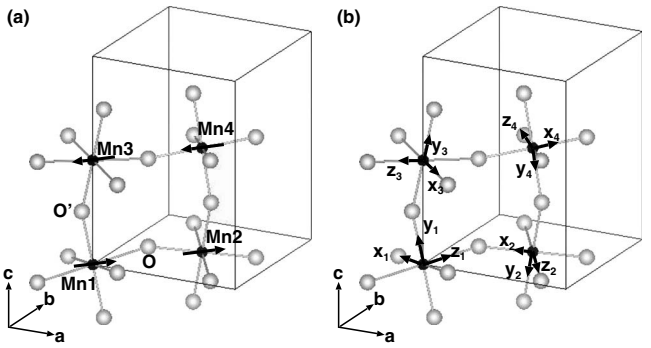

FIG. 1. (a) Sketch of the unit cell. La sites are omitted. The experimentally observed crystal and magnetic structure is assumed. The arrows on the Mn sites indicate the magnetic moment. (b) Local coordinates at each Mn site. The z_λ ($\lambda=1,\ldots,4$) axis is taken to be parallel to the longest Mn_λ-O bond, while x_λ and y_λ axes are nearly parallel to the shortest Mn_λ-O and the middle length Mn_λ-O′ bonds, respectively.

II. ELECTRONIC STRUCTURE OF $LaMnO_3$

A. Multiorbital tight-binding model

We assume the crystal and magnetic structure of $LaMnO_3$ as shown in Fig. 1(a) and also define the local coordinates x_λ, y_λ, and z_λ on the λth Mn site in a unit cell as shown in Fig. 1(b). We introduce a tight-binding model involving all Mn 3*d* orbitals and O 2*p* orbitals. We exclude orbitals belonging to the La atoms, since those orbitals play minor roles in the electronic states near the insulating gap. Thus, the model Hamiltonian is expressed as

$$H = H_0 + H_{\mathrm{I}}, \tag{1}$$

$$H_0 = \sum_{im\sigma} E_i^d n_{im\sigma}^d + \sum_{jm\sigma} E_j^p n_{jm\sigma}^p + \sum_{(i,j)} \sum_{mm'\sigma} (t_{im,jm'}^{dp} d_{im\sigma}^\dagger p_{jm'\sigma} + \mathrm{H.c.}) + \sum_{(j,j')} \sum_{mm'\sigma} (t_{jm,j'm'}^{pp} p_{jm\sigma}^\dagger p_{j'm'\sigma} + \mathrm{H.c.}), \tag{2}$$

$$H_{\mathrm{I}} = \frac{1}{2} \sum_i \sum_{\nu_1\nu_2\nu_3\nu_4} g(\nu_1,\nu_2;\nu_3,\nu_4) d_{\nu_1}^\dagger d_{\nu_2}^\dagger d_{\nu_4} d_{\nu_3}. \tag{3}$$

The part H_0 is the kinetic energy part, where $d_{im\sigma}$ and $p_{jm\sigma}$ denote the annihilation operators of an electron with spin σ in the 3*d* orbital *m* at Mn site *i* and in the 2*p* orbital *m* at O site *j*, respectively. $n_{im\sigma}^d$ and $n_{jm\sigma}^p$ are the number operators given by $d_{im\sigma}^\dagger d_{im\sigma}$ and $p_{jm\sigma}^\dagger p_{jm\sigma}$, respectively. The transfer integrals $t_{im,jm'}^{dp}$ and $t_{jm,j'm'}^{pp}$ are evaluated from the Slater-Koster (SK) two-center integrals, $(pd\sigma)$, $(pd\pi)$, $(pp\sigma)$, $(pp\pi)$.[25] We neglect the hybridization between the Mn sites. In order to take account of the JTD, we assume the $\ell^{-\alpha}$ law for the SK parameters suggested by Harrison,[26] where ℓ represents the atomic distance between neighboring sites and $\alpha=2$ for $pp\sigma$ and $pp\pi$, $\alpha=3.5$ for $pd\sigma$ and $pd\pi$. Thus, the JTD, rotation, and tilt of the MnO_6 octahedron are incorporated into the model. The part H_I represents the intra-atomic Coulomb interaction on the Mn sites. The interaction matrix element $g(\nu_1,\nu_2;\nu_3,\nu_4)$, where ν stands for spin-orbit $(m\sigma)$,

TABLE I. Tight-binding parameters in units of eV. SK parameters for the nearest Mn-O′ pair and for the nearest O-O′ pair are given in the table, while the other parameters are determined by adopting $\ell^{-\alpha}$ law suggested by Harrison (Ref. 26). Slater integral F^2 and F^4 are taken from Ref. 27.

$pd\sigma$	−2.01	F^0	5.03	U	4.5
$pd\pi$	0.93	F^2	9.74		
$pp\sigma$	0.63	F^4	6.96		
$pp\pi$	−0.18	E_d-E_p	−14.0	Δ	4.0

is written in terms of the Slater integrals F^0, F^2, and F^4. Among them, F^2 and F^4, which are known to be slightly screened by solid-state effects, are taken from the cluster model analysis of the x-ray photoemission spectroscopy.[27] On the other hand, F^0 is known to be considerably screened, so that we regard the value as an adjustable parameter. The Coulomb interaction on O sites is absorbed into a renormalization of the O $2p$ level parameters $E^p_{jm\sigma}$. The Mn d-level position relative to the O p-levels is given by the charge-transfer energy Δ defined as $\Delta=E_d-E_p+4U$ in the d^4 configuration, where U is the multiplet-averaged d-d Coulomb interaction given by $U=F^0-(2/63)F^2-(2/63)F^4$.[27] The charge-transfer energy Δ is also treated as an adjustable parameter in our calculation. The parameters used in the calculation are listed in Table I.

B. Hartree-Fock approximation

Assuming the A-type AFM order, we solve the tight-binding Schrodinger equation within the HFA. We obtain a stable A-type AFM solution, which has the energy gap ~1.0 eV and the spin moment at Mn site ~2.0 $\hbar$. The DOSs projected onto the $3z^2_\lambda-r^2$, $x^2_\lambda-y^2_\lambda$, and t_{2g} states are shown in Fig. 2, and that projected onto $2p$ states in Fig. 3. In the local coordinates, they are independent of λ $(1,\cdots,4)$. The local majority spin $3z^2_\lambda-r^2$ states are almost fully occupied and mainly concentrate on the occupied energy ranges denoted by A and C; they also concentrate on the unoccupied energy range denoted by A'. The local majority spin $x^2_\lambda-y^2_\lambda$ states are partially occupied on energy ranges denoted by A and C; they also concentrate on the unoccupied energy ranges denoted by A'. On the other hand, the local minority spin e_g states highly concentrate on the unoccupied energy range denoted by B' and C', although a small amount of them resides on the occupied energy range denoted by B. The difference in the occupation numbers between the $3z^2_\lambda-r^2$ and $x^2_\lambda-y^2_\lambda$ states implies that the e_g states are orbitally ordered, corresponding to the experimentally observed orbital order. In contrast to the e_g states, the local majority and minority spin t_{2g} states are almost perfectly occupied and unoccupied, respectively. The e_g states around the energy ranges denoted by B and C are highly hybridized with O $2p$ states. In contrast, the occupied states around the energy range denoted by A and unoccupied states denoted by A' have very small weight of the $2p$ states. This difference arises from the fact that the oxygen $2p$ states are located in the relatively deep energy region as shown in Fig. 3.

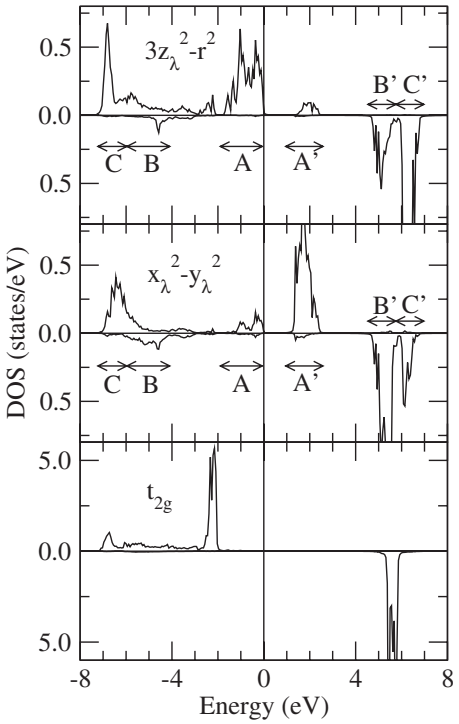

FIG. 2. DOS projected on the Mn $3z^2_\lambda-r^2$, $x^2_\lambda-y^2_\lambda$, and t_{2g} states. The origin of energy is at the top of valence band. In each panel the upper half represents the DOS for the local majority spin and the lower one for the local minority spin.

$LaMnO_3$ is close not to the charge-transfer-type insulator but to the Mott-Hubbard-type insulator.

The dispersion curves along some symmetric lines near the gap are shown in Fig. 4. Labels assigned to the curves correspond to the states shown in the Fig. 3. The curves corresponding to the states denoted by A and A' well reproduce those calculated with the *ab initio* band-structure calculation based on the LDA+U method[28] except for the magnitude of the gap.

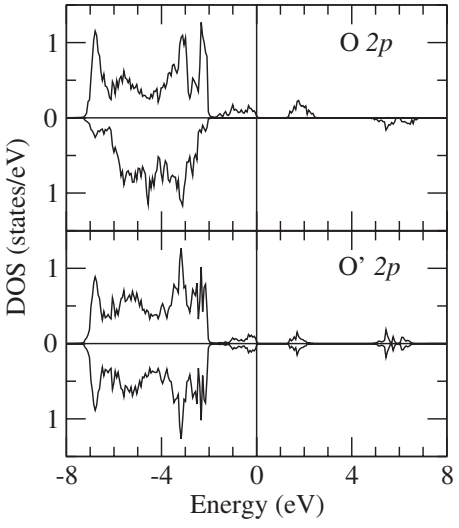

FIG. 3. DOS projected on the O $2p$ states at the sites denoted by O and O′ in Fig. 1. The origin of energy is at the top of valence band.

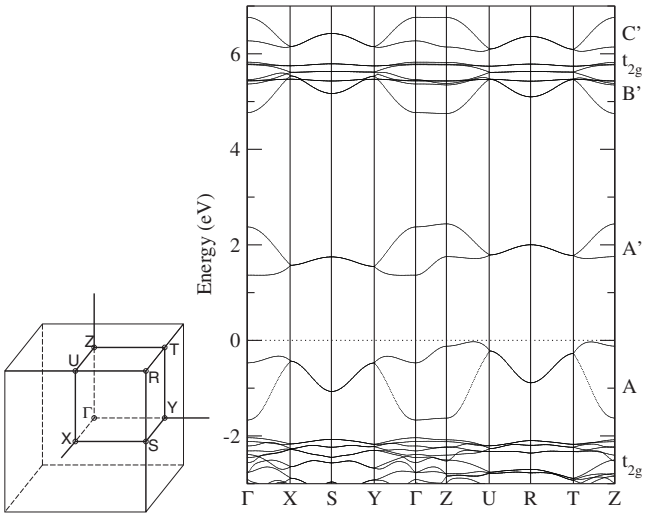

FIG. 4. Dispersion curves along the several symmetric lines vicinity of the gap. The origin of energy is at the top of valence band.

III. RIXS PROCESS

We briefly summarize the NI formula for the RIXS, following Ref. 23. In the RIXS process, the incident photon is absorbed by exciting a Mn $1s$ core electron to the unoccupied $4p$ state, and a photon is emitted by recombining the $4p$ electron and the core hole. This process may be described by

$$H_x = w\sum_{\mathbf{q}\alpha}\frac{1}{\sqrt{2\omega_{\mathbf{q}}}}\sum_{i\eta\sigma} e_\eta^{(\alpha)} p'^{\dagger}_{i\eta\sigma} s_{i\sigma} c_{\mathbf{q}\alpha} e^{i\mathbf{q}\cdot\mathbf{r}_i} + \text{H.c.}, \tag{4}$$

where w represents the dipole transition matrix element between the $1s$ and the $4p$ states. We assume that w is constant, since it is expected to change little in the energy range of 20 eV above the absorption edge. It is known that the energy dependence of w gives minor effect on the Cu K-edge absorption spectra.[21] The e_η represents the ηth component ($\eta = x,y,z$) of the photon polarization vector. Annihilation operators $p'_{i\eta\sigma}$ and $s_{i\sigma}$ are for states $4p_\eta$ and state $1s$ with spin σ at Mn site i, respectively. The annihilation operator $c_{\mathbf{q}\alpha}$ is for photon with momentum $\mathbf{q}$ and polarization $e_\eta^{(\alpha)}$. In the intermediate state of the RIXS process, the core-hole potential is acting on the $3d$ states, creating an electron-hole pair within the Born approximation. The interaction is described as

$$H_{1s\text{-}3d} = V\sum_{im\sigma\sigma'} d^{\dagger}_{im\sigma} d_{im\sigma} s^{\dagger}_{i\sigma'} s_{i\sigma'}, \tag{5}$$

where i runs over Mn sites. Note that although the value of the core-hole interaction V is not known and may strongly depend on the model, it is expected to be much larger than the $4p$-$3d$ off-diagonal Coulomb interaction. In the end of the process, an electron-hole pair is left behind carrying momentum energy $q \equiv (\mathbf{q},\omega) = (\mathbf{q}_i - \mathbf{q}_f, \omega_i - \omega_f)$, where $q_i = (\mathbf{q}_i, \omega_i)$ and $q_f = (\mathbf{q}_f, \omega_f)$ are momentum energies of incident and scattered photons, respectively.

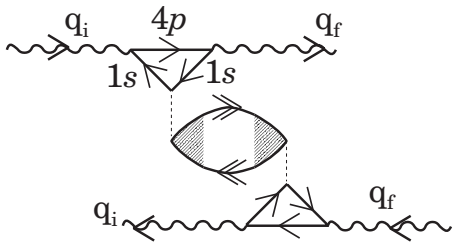

FIG. 5. Diagram for the RIXS intensity within the Born approximation for the $1s$ core-hole potential. The wavy and dotted lines represent photon Green's functions and the core-hole interaction V, respectively. The solid lines with the labels $4p$ and $1s$ represent the bare Green's functions for the $4p$ electron and the $1s$ core electron, respectively. The elliptic part between the core-hole interaction lines corresponds to the density-density correlation function of the Keldysh type. The lines with double arrows are the Keldysh-type Green's functions. The shaded area represents the effective scattering vertex renormalized by $3d$-$3d$ Coulomb interaction in the RPA.

The RIXS intensity is derived on the basis of the Keldysh-Green's function scheme. It is diagrammatically represented in Fig. 5. Within the Born approximation for the core-hole potential, we obtain

$$W(q_i,\mathbf{e}_i;q_f,\mathbf{e}_f) = \frac{N|w|^4}{4\omega_i\omega_f}\sum_{\lambda m\sigma}\sum_{\lambda' m'\sigma'} e^{i\mathbf{q}\cdot(\mathbf{u}_\lambda - \mathbf{u}_{\lambda'})} \times Y^{+-}_{\lambda m\sigma,\lambda' m'\sigma'}(q) J_{B\lambda\lambda'}(\omega_i,\mathbf{e}_i;\omega_f,\mathbf{e}_f), \tag{6}$$

where λ indicates the λth Mn site in a unit cell, and $\mathbf{u}_\lambda$ represents the position vectors of the λth Mn site in a unit cell. N is the number of unit cells. The factor $J_{B\lambda\lambda'}(\omega_i,\mathbf{e}_i;\omega_f,\mathbf{e}_f)$ describes the incident-photon dependence, which is given by

$$J_{B\lambda\lambda'}(\omega_i,\mathbf{e}_i;\omega_f,\mathbf{e}_f) = \left(\sum_{\eta\eta'} e_{i\eta} L^{\eta\eta'}_{B\lambda}(\omega_i;\omega_f) e_{f\eta'}\right) \times \left(\sum_{\eta\eta'} e_{i\eta} L^{\eta\eta'}_{B\lambda'}(\omega_i;\omega_f) e_{f\eta'}\right)^*, \tag{7}$$

where $e_{i\eta}$ ($e_{f\eta}$) is the ηth component of the polarization vector $\mathbf{e}_i$ ($\mathbf{e}_f$) with $\eta = x,y,z$, and $L^{\eta\eta'}_{B\lambda}(\omega_i;\omega)$ is given by

$$L^{\eta\eta'}_{B\lambda}(\omega_i;\omega_f) = \frac{V}{N}\int_{\epsilon_0}^{\infty} \frac{\rho^{\eta\eta'}_{\lambda 4p}(\epsilon)d\epsilon}{(\omega_i + \epsilon_{1s} + i\Gamma_{1s} - \epsilon)(\omega_f + \epsilon_{1s} + i\Gamma_{1s} - \epsilon)}. \tag{8}$$

The Γ_{1s} represents the lifetime broadening width of the core-hole state, and the lower limit of the integral ϵ_0 indicates the energy at the bottom of the $4p$ band. This expression comes from the upper triangle in Fig. 5. The $\rho^{\eta\eta'}_{\lambda 4p}$ is the DOS matrix in the p symmetric states at the λth Mn site, which may be given by

$$\rho^{\eta\eta'}_{\lambda 4p}(\epsilon) = \sum_\sigma\sum_{n\mathbf{k}} \phi^*_{\lambda\eta\sigma}(n,\mathbf{k})\phi_{\lambda\eta'\sigma}(n,\mathbf{k})\delta[\epsilon - \epsilon_n(\mathbf{k})], \tag{9}$$

where $\phi_{\lambda\eta\sigma}(n,\mathbf{k})$ is the amplitude of p_η component with spin σ at the λth Mn site in the band state specified by the band

index n and crystal momentum $\mathbf{k}$ with energy $\epsilon_n(\mathbf{k})$. The factor $Y^{+-}_{\lambda' m'\sigma',\lambda m\sigma}(q)$ in Eq. (6) is the density-density correlation function of the Keldysh type, which is defined by

$$Y^{+-}_{\lambda' m'\sigma',\lambda m\sigma}(\mathbf{q},\omega) = \int_{-\infty}^{\infty} \langle (\rho_{\mathbf{q}\lambda' m'\sigma'})^{\dagger}(\tau)\rho_{\mathbf{q}\lambda m\sigma}(0)\rangle e^{i\omega\tau} d\tau, \tag{10}$$

where

$$\rho_{\mathbf{q}\lambda m\sigma} = \sqrt{\frac{4}{N}} \sum_{\mathbf{k}} d^{\dagger}_{\mathbf{k}+\mathbf{q}\lambda m\sigma} d_{\mathbf{k}\lambda m\sigma}, \tag{11}$$

with

$$d_{\mathbf{k}\lambda m\sigma} = \sqrt{\frac{4}{N}} \sum_{n} d_{n\lambda m\sigma} e^{i\mathbf{k}\cdot\mathbf{r}_n}. \tag{12}$$

The index $\lambda m\sigma$ specifies a tight-binding orbital at site λ with orbital m and spin σ; λ (=1,2,3,4) is assigned to four Mn sites in a unit cell. Wave vector $\mathbf{k}$ in Eq. (11) runs over the first Brillouin zone. Vector $\mathbf{r}_n$ in Eq. (12) represents a position vector of the nth unit cell. A single phase factor $\mathbf{k}\cdot\mathbf{r}_n$ is assigned to all the $3d$ states in each unit cell, and hence an extra factor $e^{i\mathbf{q}\cdot(\mathbf{u}_\lambda - \mathbf{u}_{\lambda'})}$ is required in Eq. (6).

We calculate the density-density correlation function (10) at zero temperature with taking account of the correlation effect on the electron-hole pair by the RPA. Abbreviating the indices $\lambda m\sigma$ as ξ, it may be written as

$$Y^{+-}_{\xi'\xi}(q) = \sum_{\xi_1'\xi_2'} \sum_{\xi_1\xi_2} \Lambda^{*}_{\xi_1'\xi_2',\xi'}(q)\Pi^{+-(0)}_{\xi_1'\xi_2',\xi_1\xi_2}(q)\Lambda_{\xi_1\xi_2,\xi}(q), \tag{13}$$

where

$$\Pi^{+-(0)}_{\xi_1\xi_2,\xi_1'\xi_2'}(q) = \frac{2\pi}{N} \sum_{\mathbf{k}} \sum_{j,j'} \delta[\omega - E_{j'}(\mathbf{k}+\mathbf{q}) + E_j(\mathbf{k})] \times [1 - n_{j'}(\mathbf{k}+\mathbf{q})] n_j(\mathbf{k}) \varphi_{\xi_1,j'}(\mathbf{k}+\mathbf{q}) \times \varphi^{*}_{\xi_1',j'}(\mathbf{k}+\mathbf{q}) \varphi_{\xi_2',j}(\mathbf{k}) \varphi^{*}_{\xi_2,j}(\mathbf{k}). \tag{14}$$

$E_j(\mathbf{k})$ and $n_j(\mathbf{k})$ are the eigenenergy and the occupation number of the eigenstate specified by $j\mathbf{k}$, respectively. The $\varphi_{\lambda m\sigma,j}(\mathbf{k})$ represents the amplitude of the $3d$ orbital and spin $m\sigma$ at the Mn site λ in the energy eigenstate specified by $j\mathbf{k}$ within the HFA. The RPA vertex $\Lambda_{\xi_1\xi_2,\xi}(q)$ is given by

$$\Lambda_{\xi_1\xi_2,\xi}(q) = [\hat{I} - \hat{\Gamma}\hat{F}^{--}(q)]^{-1}_{\xi_1\xi_2,\xi\xi}, \tag{15}$$

where $\hat{I}$ represents a unit matrix, and $\hat{\Gamma}$ is the bare four-point antisymmetric vertex given by

$$[\hat{\Gamma}]_{\xi_1\xi_2,\xi_3\xi_4} = [g(\nu_1\nu_2;\nu_3\nu_4) - g(\nu_1\nu_2;\nu_4\nu_3)]\delta_{\lambda_1\lambda_2}\delta_{\lambda_3\lambda_4}\delta_{\lambda_1\lambda_3}. \tag{16}$$

The two-particle propagator $\hat{F}^{--}(q)$ is given by

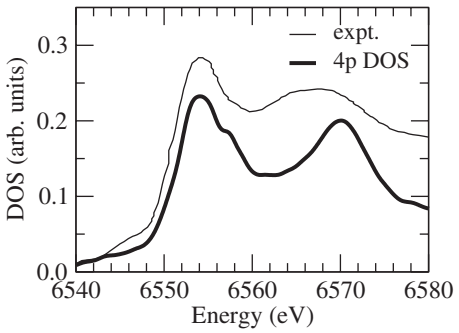

FIG. 6. The LDA $4p$ DOS convoluted by the Lorentzian function with FWHM $2\Gamma_{1s}$=2 eV (thick solid curve). In connection with the absorption coefficient, the origin of energy is shifted so that the prominent peak locates at 6554 eV. Thin curve is the absorption spectra reproduced from Ref. 32.

$$[\hat{F}^{--}(q)]_{\xi_1\xi_2,\xi_3\xi_4} = \frac{1}{N} \sum_{jj'} \sum_{\mathbf{k}} \varphi_{\xi_4,j}(\mathbf{k})\varphi^{*}_{\xi_2,j}(\mathbf{k}) \times \varphi_{\xi_1,j'}(\mathbf{k}+\mathbf{q})\varphi^{*}_{\xi_3,j'}(\mathbf{k}+\mathbf{q}) \times \left\{ \frac{n_j(\mathbf{k})[1 - n_{j'}(\mathbf{k}+\mathbf{q})]}{\omega - E_{j'}(\mathbf{k}+\mathbf{q}) + E_j(\mathbf{k}) + i\delta} - \frac{n_{j'}(\mathbf{k}+\mathbf{q})[1 - n_j(\mathbf{k})]}{\omega - E_{j'}(\mathbf{k}+\mathbf{q}) + E_j(\mathbf{k}) - i\delta} \right\}. \tag{17}$$

We evaluate the density-density correlation function (10) using Eqs. (13)–(17). For more details of the derivation, see Refs. 21–23. Note that the terms involving $\Pi^{-+(0)}(q)$ are neglected; they have no contribution for $\omega > 0$ at zero temperature, because $\Pi^{-+(0)}(q) \propto \Sigma_{\mathbf{k}}[1-n(\mathbf{k})]n(\mathbf{k}+\mathbf{q})\delta[\omega - E_{j'}(\mathbf{k}+\mathbf{q}) + E_j(\mathbf{k})]$ with omitting unimportant factors.

IV. CALCULATED RESULTS

In order to calculate the incident-photon-dependent factor $J_{B\lambda\lambda'}(\omega_i, \mathbf{e}_i; \omega_f, \mathbf{e}_f)$, we need the $4p$ DOS $\rho^{\eta\eta'}_{\lambda 4p}(\epsilon)$ on the λth Mn site. We evaluate the $4p$ DOS using full potential linear augmented plane-wave band-structure calculation based on the LDA+U method. It should be noted here that the Mn $4p$ DOS depends on η, η' and on Mn site λ due to the strong JTD, giving rise to the Mn K-edge resonant elastic x-ray scattering intensity on forbidden Bragg spots.[29–31] Figure 6 shows the $4p$ DOS averaged with η ($\Sigma_\eta \rho^{\eta\eta}_{\lambda 4p}(\epsilon)$) and convoluted with a Lorentzian function of FWHM $2\Gamma_{1s}$=2 eV, in comparison with the absorption experiment.[32] We set the energy difference between the Mn $1s$ level and the prominent peak in the $4p$ DOS to be 6554 eV. Under the condition that the dipole matrix element is constant and that the interaction is neglected between the core hole and the $4p$ electron, the $4p$ DOS becomes proportional to the Mn K-edge absorption spectra. The agreement with the experiment indicates that the above condition is nearly satisfied.

Equations (6)–(8) indicate that the photon polarization dependence of the RIXS intensity correlates only with the Mn $4p$ states. Therefore, the polarization dependence would

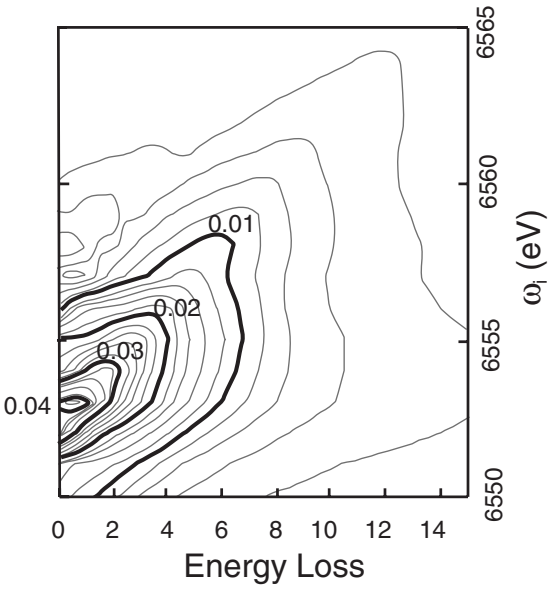

FIG. 7. Contour plot of $J_A(\omega_i;\omega_f)$ as a function of energy loss $\omega=\omega_i-\omega_f$ and incident-photon energy ω_i. $2\Gamma_{1s}=2$ eV. Units of the intensity are arbitrary.

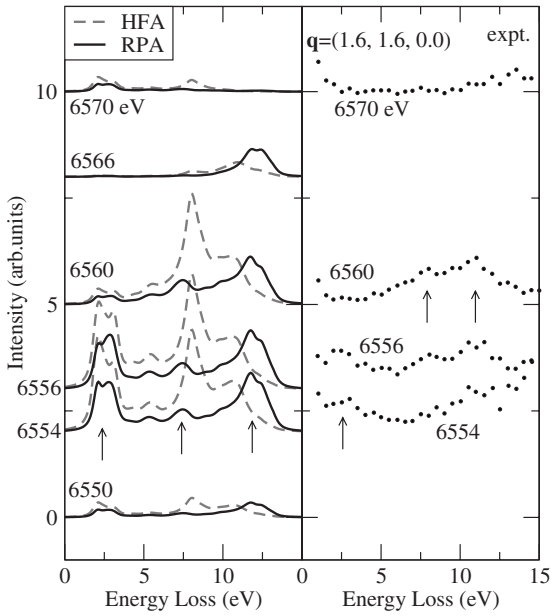

FIG. 8. RIXS spectra at $\mathbf{q}=(1.6,1.6,0.0)$ as a function of energy loss for several incident-photon energies. Calculated RIXS spectra are shown in the left panel and the observed spectra reproduced from Ref. 12 in the right panel. The solid and dashed curves are spectra calculated by including the RPA correction and within the HFA, respectively. The incident-photon energies are shown besides each spectral curve in units of eV. Arrows indicate characteristic features in the spectra.

not have relevant information on the charge excitations in the $3d$ states. Hence, we will not touch on the polarization dependence. Assuming polarization-unresolved analysis, we neglect the off-diagonal elements of the $4p$ DOS matrix and replace each diagonal element with the averaged value for simplicity. Accordingly, the factor $J_{B\lambda\lambda'}(\omega_i,\mathbf{e}_i;\omega_f,\mathbf{e}_f)$ is replaced with the averaged site-independent factor $J_A(\omega_i;\omega_f)\sim|\Sigma_\eta L_B^{\eta\eta}(\omega_i;\omega_f)|^2$. Figure 7 shows the contour plot of $J_A(\omega_i;\omega_f)$ as a function of incident-photon energy ω_i and energy loss $\omega=\omega_i-\omega_f$. The enhancement appears around the energy loss of 2 eV for the incident-photon energy around 6554 eV. As the incident-photon energy increases, the enhancement peak moves toward higher energy-loss region with decreasing the intensity. It is expected that the factor $J_{B\lambda\lambda'}(\omega_i,\mathbf{e}_i;\omega_f,\mathbf{e}_f)$ has dependence similar to the factor $J_A(\omega_i;\omega_f)$, although the enhancement peak position and the intensity may somewhat depend on the photon polarization.

Another factor $Y^{+-}_{\lambda' m'\sigma,\lambda m\sigma}(q)$ mainly determines the structure of the RIXS spectra as a function of energy loss. We calculate this factor from Eqs. (10)–(17) using the tight-binding wave function within the HFA and by including the RPA correction. The transition from the occupied e_g states in the energy ranges denoted by A, B, and C to the unoccupied e_g states in those denoted by A', B', and C' can be driven due to the $1s$ core-hole potential, because the occupied states and the unoccupied states comprise the e_g states with the same local symmetry. Therefore, the e_g states can contribute to the RIXS intensity. In contrast to the e_g states, the t_{2g} states cannot contribute to the RIXS intensity, since the local majority and minority spin t_{2g} states are almost perfectly occupied and unoccupied, respectively, and the spin-flip transition is not allowed.

Combining two factors, we obtain the RIXS spectra. We convolute the result with a Lorentzian function of FWHM $=0.5$ eV for taking account of the instrumental resolution.

Figure 8 shows the spectra thus evaluated at the momentum transfer $\mathbf{q}=(1.6,1.6,0.0)$ as a function of energy loss for several incident-photon energies in comparison with the experiments.[12–14] We obtain continuous spectra ranging from $\omega=2$ to 15 eV within the HFA; there are three features around $\omega=2.5$, 7.5, and 12 eV, which arise from transitions of $A\rightarrow A'$, $C\rightarrow A'$ in the local majority spin channel, and $B\rightarrow B'$, C' in the local minority spin channel, respectively, within the e_g states (see Figs. 2 and 4). As already stated, the t_{2g} states could not contribute to the RIXS intensity. The spectral shape within the HFA is drastically modified by the RPA correction; the intensity around the energy loss $\omega\sim2.5$ and 8 eV is suppressed and that around $\omega\sim12$ eV is enhanced. The spectral shape thus modified corresponds well to the experimentally observed features at $\omega=2.5$, 8, and 11 eV. Another characteristic is that the weight of the RIXS intensity moves toward higher energy-loss region as the incident-photon energy increases. This change is nicely reproduced by the calculation, mainly due to the effect of the incident-photon-energy factor J_A. Figure 9 shows another comparison with the experiment at other momentum transfers $\mathbf{q}=(2.7,0.0,0.0)$ and $(4.5,0.0,0.0)$.[13] The calculated spectra agree with the experiment.

Figure 10 shows a contour plot of RIXS spectra as a function of energy loss and momentum transfer $\mathbf{q}$ along $(0,0,0)-(2,0,0)$, $-(0,2,0)$, $-(0,0,2)$, and $-(2,2,0)$ lines. The incident-photon energy ω_i is fixed at 6556 eV. Three ridges around the energy loss 2.5, 7.5, and 12 eV correspond to the three peaks around the energy loss 2.5, 7.5, and 12 eV, respectively, in Figs. 8 and 9. The peak *position* only slightly

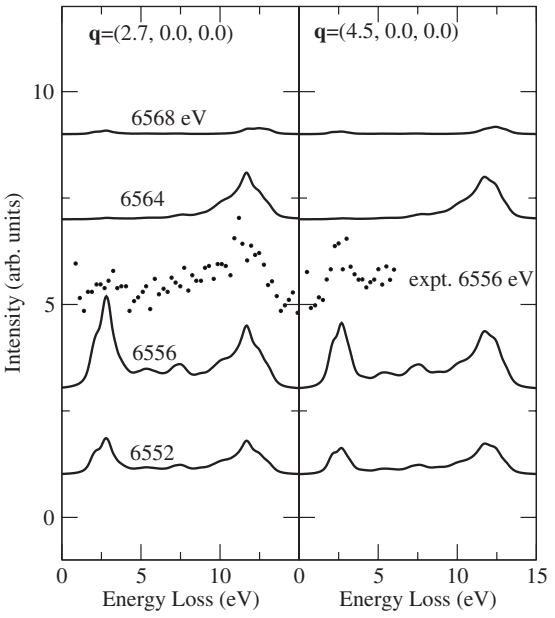

FIG. 9. RIXS spectra at $\mathbf{q}=(2.7,0.0,0.0)$ and $(4.5,0.0,0.0)$ as a function of energy loss for several incident-photon energies. The solid curves represent the spectra calculated by including the RPA correction. Dotted ones are the observed spectra at $\hbar\omega_i=6556$ eV reproduced from Ref. 13.

depends on the momentum transfer $\mathbf{q}$, moving within ~ 1 eV. This is consistent with the experiments and may be due to the fact that the states relevant to the RIXS process concentrate on the narrow energy ranges. Note that the peaks at 2.5, 7.5, and 12 eV correspond to transitions $A \rightarrow A'$, $C \rightarrow A'$ in the local majority spin channel, and $B \rightarrow B'$, C' in the local minority spin channel, respectively (see Figs. 2 and 4). In contrast, the peak *intensity* noticeably depends on the momentum transfer showing the period of 2 along the a, b, and c directions, although this fact has not been emphasized in the experiments.[12–14] It does not seem easy, however, to explain the origin of this dependence, since the intensities depend sensitively on the $3d$ weights in the energy bands [see Eq. (14)]. Different from the present case, the peak positions as a function of energy loss have been found clearly moving with varying momentum transfer in La_2CuO_4 in the high-resolution experiments.[7–11] It should be noted here that the peak shift with varying momentum transfer should not be interpreted as a dispersion relation of a kind of exciton but as a change in spectral weight in the continuum spectra. The crystal momentum dependence of the weight of the states relevant to the RIXS process and the energy dispersion of the single electron states determine the momentum transfer dependence of the RIXS intensity.

V. CONCLUDING REMARKS

We have analyzed the incident-photon-energy and momentum dependence on the RIXS spectra as a function of energy loss in $LaMnO_3$. We have utilized the formula developed by Nomura and Igarashi, which expresses the RIXS spectra by a product of the photon dependent factor and the density-density correlation function. The former factor, which describes the dependence on the incident-photon en-

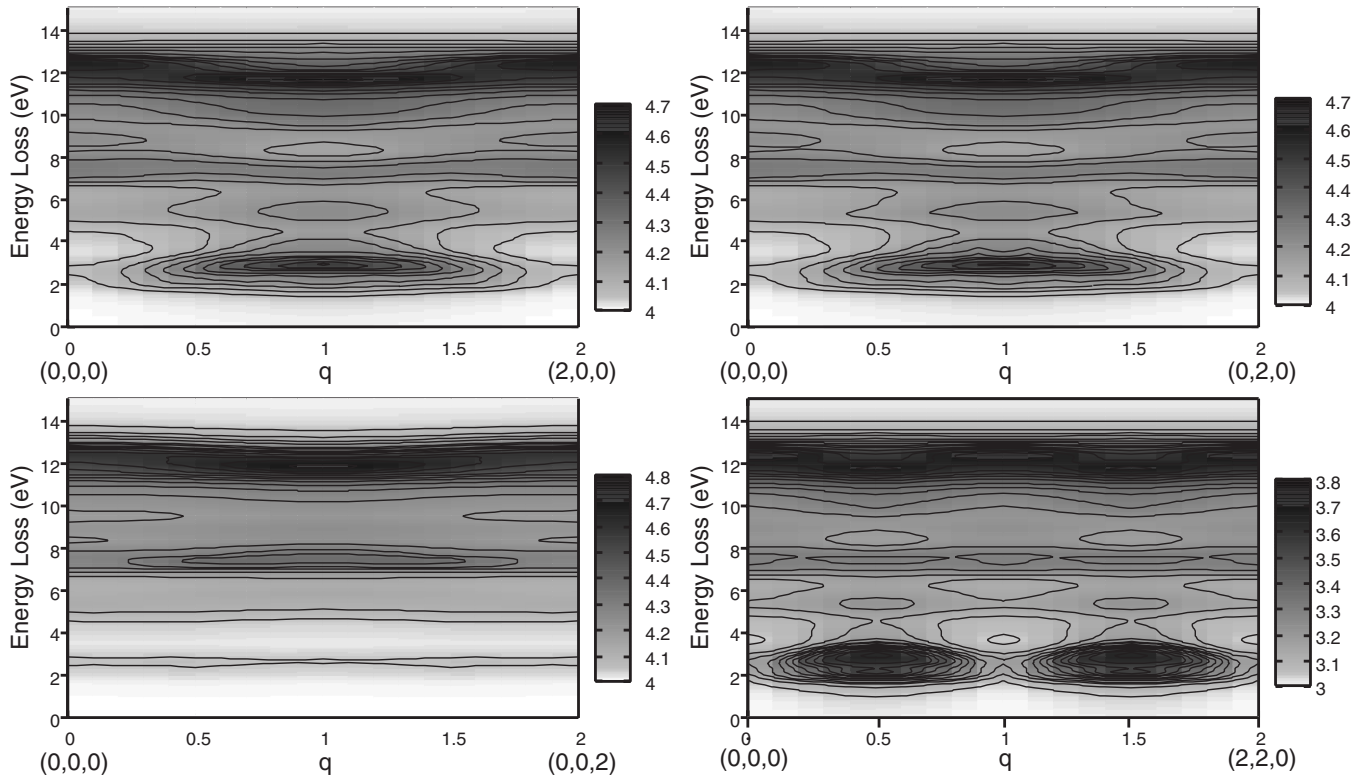

FIG. 10. RIXS spectra as a function of momentum transfer $\mathbf{q}$ along $(0,0,0)-(2,0,0)$, $-(0,2,0)$, $-(0,0,2)$, and $-(2,2,0)$ lines. *Pbnm* setting is assumed for the definition of $\mathbf{q}$. The incident-photon energy is fixed at $\omega_i=6556$ eV. The unit of the intensity is arbitrary.

ergy and polarization, has been calculated by using the Mn $4p$ DOS given by the *ab initio* band-structure calculation. The latter function describes the charge excitations generated in the $3d$ states to screen the core-hole potential in the intermediate state.

Having combined the above factors, we have calculated the RIXS spectra as a function of energy loss. We have obtained a continuous spectrum consisting of three features in good agreement with the experiments. We have found that the RPA correlation modifies drastically the spectral shape, which indicates the importance of electron correlations for making quantitative analysis. We have demonstrated that the peak intensity depends strongly on the momentum transfer $\mathbf{q}$ with the periodicity 2 along the a, b, and c directions while the three peak positions as a function of energy loss only slightly depend on $\mathbf{q}$. Furthermore, we have obtained the spectral weight moving toward high energy-loss region with increasing incident-photon energy, in agreement with the experiments.

The present analysis naturally leads to a RIXS picture that the spectra are brought about by band-to-band transitions (augmented by the RPA correction) in order to screen the core-hole potential. This picture is different from a previous picture that the spectra are brought about by $3d$ orbital excitations (orbitons) created with the use of the off-diagonal part of the Coulomb interaction between the photoexcited $4p$ electron and $3d$ electrons.[12,15] This "orbiton" picture seems unreasonable, since the $4p$-$3d$ off-diagonal Coulomb interaction, which causes orbitons, is much smaller than the $1s$-$3d$ Coulomb interaction, which causes band-to-band transitions. Actually the "orbiton" picture was not successful in providing the spectra comparable to the experiment.[12] Note that the two pictures give different selection rules for the creation of excitation; the present picture forbids the transition from $3z^2-r^2$-type orbital to the x^2-y^2-type orbital, while the latter allows it by changing $4p$ states.

For doped cuprates and manganites, experimental data have been accumulated.[13,14] In doped cuprates the RIXS spectra have been analyzed by the same formula as the present one within the HFA.[33] As already demonstrated in Refs. 16, 17, and 21–23, the HFA alone, without taking account of the RPA correlation, is not sufficient for quantitative understanding of the spectra even in the undoped materials. In doped materials, electron correlations may become more important, and the HFA-RPA scheme would not work well. Also, the Born approximation may be insufficient for treating the core-hole potential, since many electron-hole pairs could be created in the absence of the energy gap. It seems hard to answer these questions by analyses with a detailed model like the present paper, and such studies are left for the future.

ACKNOWLEDGMENTS

This work was partially supported by a Grant-in-Aid for Scientific Research from the Ministry of Education, Culture, Sports, Science, and Technology of Japan.

[1] J. B. A. A. Elemans, B. Van Laar, K. R. Van Der Veen, and B. O. Loopstra, J. Solid State Chem. **3**, 238 (1971).
[2] C. Ritter, M. R. Ibarra, J. M. De Teresa, P. A. Algarabel, C. Marquina, J. Blasco, J. García, S. Oseroff, and S.-W. Cheong, Phys. Rev. B **56**, 8902 (1997).
[3] J. Kanamori, J. Appl. Phys. **31**, S14 (1960).
[4] K. I. Kugel and D. I. Khomskii, JETP Lett. **15**, 446 (1972).
[5] E. O. Wollan and W. C. Koehler, Phys. Rev. **100**, 545 (1955).
[6] G. Matsumoto, J. Phys. Soc. Jpn. **29**, 606 (1970).
[7] M. Hasan, E. Isaacs, Z.-X. Shen, L. L. Miller, L. Tsutsui, T. Tohyama, and S. Maekawa, Science **288**, 1811 (2000).
[8] Y. J. Kim, J. P. Hill, C. A. Burns, S. Wakimoto, R. J. Birgeneau, D. Casa, T. Gog, and C. T. Venkataraman, Phys. Rev. Lett. **89**, 177003 (2002).
[9] S. Suga, S. Imada, A. Higashiya, A. Shigemoto, S. Kasai, M. Sing, H. Fujiwara, A. Sekiyama, A. Yamasaki, C. Kim, T. Nomura, J. Igarashi, M. Yabashi, and T. Ishikawa, Phys. Rev. B **72**, 081101(R) (2005).
[10] L. Lu, J. N. Hancock, G. Chabot-Couture, K. Ishii, O. P. Vajk, G. Yu, J. Mizuki, D. Casa, T. Gog, and M. Greven, Phys. Rev. B **74**, 224509 (2006).
[11] D. S. Ellis, J. P. Hill, S. Wakimoto, R. J. Birgeneau, D. Casa, T. Gog, and Y. J. Kim, Phys. Rev. B **77**, 060501(R) (2008).
[12] T. Inami *et al.*, Phys. Rev. B **67**, 045108 (2003).
[13] K. Ishii *et al.*, Phys. Rev. B **70**, 224437 (2004).
[14] S. Grenier *et al.*, Phys. Rev. Lett. **94**, 047203 (2005).
[15] H. Kondo, S. Ishihara, and S. Maekawa, Phys. Rev. B **64**, 014414 (2001).
[16] T. Nomura and J. Igarashi, J. Phys. Soc. Jpn. **73**, 1677 (2004).
[17] T. Nomura and J. Igarashi, Phys. Rev. B **71**, 035110 (2005).
[18] P. Nozières and E. Abrahams, Phys. Rev. B **10**, 3099 (1974).
[19] L. V. Keldysh, Sov. Phys. JETP **20**, 1018 (1965).
[20] P. Abbamonte, C. A. Burns, E. D. Isaacs, P. M. Platzman, L. L. Miller, S. W. Cheong, and M. V. Klein, Phys. Rev. Lett. **83**, 860 (1999).
[21] J.-i. Igarashi, T. Nomura, and M. Takahashi, Phys. Rev. B **74**, 245122 (2006).
[22] M. Takahashi, J. Igarashi, and T. Nomura, J. Phys. Soc. Jpn. **77**, 034711 (2008).
[23] M. Takahashi, J. Igarashi, and T. Nomura, Phys. Rev. B **75**, 235113 (2007).
[24] P. Nozières and C. T. D. Dominicis, Phys. Rev. **178**, 1097 (1969).
[25] J. C. Slater and G. F. Koster, Phys. Rev. **94**, 1498 (1954).
[26] W. A. Harrison, *Electronic Structure and the Properties of Solids: The Physics of the Chemical Bond* (Freeman, San Francisco, 1980).
[27] A. E. Bocquet, T. Mizokawa, T. Saitoh, H. Namatame, and A. Fujimori, Phys. Rev. B **46**, 3771 (1992).
[28] H. Sawada, Y. Morikawa, K. Terakura, and N. Hamada, Phys. Rev. B **56**, 12154 (1997).
[29] I. S. Elfimov, V. I. Anisimov, and G. A. Sawatzky, Phys. Rev. Lett. **82**, 4264 (1999).

[30] M. Benfatto, Y. Joly, and C. R. Natoli, Phys. Rev. Lett. **83**, 636 (1999).
[31] M. Takahashi, J. Igarashi, and P. Fulde, J. Phys. Soc. Jpn. **68**, 2530 (1999).
[32] G. Subías, J. García, M. G. Proietti, and J. Blasco, Phys. Rev. B **56**, 8183 (1997).
[33] R. S. Markiewicz and A. Bansil, Phys. Rev. Lett. **96**, 107005 (2006).